Vector and tensor analyzing powers in the $^{208}Pb(\vec{d},t)^{207}Pb$ reaction at 200 and 360 MeV

J. Van de Wiele,[1] H. Langevin-Joliot,[1] J. Guillot,[1] L. H. Rosier,[1] A. Willis,[1] M. Morlet,[1]
G. Duhamel-Chretien,[2] E. Gerlic,[3] E. Tomasi-Gustafsson[4]
N. Blasi,[5] S. Micheletti,[5] and S. Y. Van der Werf[6]
[1]*Institut de Physique Nucléaire, Boîte Postale No. 1, 91406 Orsay, France*
[2]*Institut des Sciences Nucléaires, 53 Avenue des Martyrs, 38026 Grenoble, France*
[3]*Institut de Physique Nucleaire, 43 boulevard du 11 Novembre, 69622 Lyon-Villeurbanne, France*
[4]*Laboratoire National Saturne, Centre d'Etudes Nucléaires–Saclay, F-91191, Gif-sur-Yvette CEDEX, France*
[5]*Istituto Nazionale di Fisica Nucleaire and University of Milan, Physics Department, Via Celoria 16, Milan 20133, Italy*
[6]*Kernfysisch Versneller Instituut, 9747 AA Groningen, The Netherlands*
(Received 9 December 1991; revised manuscript received 14 February 1992)

Cross sections and vector and tensor analyzing powers for the main levels in ^{207}Pb have been measured via the $^{208}Pb(\vec{d},t)^{207}Pb$ reaction at 200 and 360 MeV incident energies. A_y and A_{yy} spin observables allow a clear identification of the valence levels, especially at 200 MeV. The results are compared with finite range distorted-wave Born approximation calculations using the Paris projectile-ejectile form factor including the S and D components. The analysis shows a large effect of the D component on the tensor analyzing powers at the most forward angles. At both energies, the spin part of the deuteron optical potential is very important to describe the analyzing powers and especially A_{yy}. A good description of all observables at 200 MeV allows this reaction to be used as a spectroscopic tool.

PACS number(s): 25.40.Hs, 24.70.+s

I. INTRODUCTION

Pickup reactions have long been used to determine the orbital angular momentum l of the single hole component of nuclear wave functions. At low incident energy this determination relies on the angular distribution of the cross sections, especially on the location of the first maximum. Such characteristic dependence is more or less lost in the reactions induced by high energy projectiles (≥ 70 MeV), which are, however, necessary to investigate high-lying states in the residual nuclei. On the other hand such high energy pickup reactions are strongly selective of large l transfers over the whole range of excitation energies. This property has proved to be quite useful in the investigation of deep hole states [1].

Besides, it is well known that the angular distribution of the vector analyzing power A_y gives some additional information about the total angular momentum j of the transferred nucleon. Using vector polarized beam essentially, the $(\vec{p},d)$, $(\vec{d},t)$, or $(\vec{d},{}^3He)$ experiments have been mainly performed with low or medium incident energy beams ($E<70$ MeV) on light to medium nuclei ($A\approx 120$). Under these conditions, the identification of $j=l+\frac{1}{2}$ vs $j=l-\frac{1}{2}$ states is best achieved for the small l values.

At the incident energy of 79.4 MeV, the $^{206}Pb(\vec{d},{}^3He)^{205}Tl$ reaction [2] has proved to be a powerful spectroscopic tool for the $l=2$ transitions. On the other hand, distorted-wave Born approximation (DWBA) analysis at higher incident energies ($E\approx 90$ MeV), has difficulties in reproducing the data of $(\vec{d},t)$ and $(\vec{d},{}^3He)$ reactions on light and medium nuclei [3].

At energies around and beyond 90 MeV [4–6] most efforts have concentrated, up to now, on the $(\vec{p},d)$ reaction with special attention on l transfer lower than or equal to 3, even on ^{208}Pb target [5]. It has been shown, especially at 200 MeV [6] on light-medium nuclei, that the specific features of cross sections and A_y angular distributions are poorly or not reproduced even with exact finite range DWBA calculations. On the other hand, the j dependence of the tensor analyzing power A_{yy}, in addition to the usual vector analyzing power A_y, has been recently observed at $E_d=16.2$ MeV for transitions induced by $(\vec{d},t)$ and $(\vec{d},{}^3He)$ reactions on s-d shell nuclei [7].

In the present work we investigate the properties of the $(\vec{d},t)$ reaction at much higher incident energies, namely at $E_d=200$ and 360 MeV with a vector and tensor polarized deuteron beam, in order to gain new information on large l neutron hole states, especially in the inner shells [8]. This paper deals with the experimental results and the analysis of the cross sections, vector and tensor analyzing powers measured for reference levels in the $^{208}Pb(\vec{d},t)^{207}Pb$ reaction. The first $1i_{13/2}$, $1h_{9/2}$, $2f_{5/2}$, and $2f_{7/2}$ valence levels, which have large spectroscopic factors and the largest cross sections, are well suited to check the DWBA description of the reaction at these two energies. The cross section angular distributions are nearly exponentially decreasing with angle, but the vector and tensor analyzing powers are found to exhibit very characteristic features, especially at $E_d=200$ MeV. These characteristic features have been used to analyze higher-lying excited groups or structures in ^{207}Pb, both in the region of valence and inner hole states. These last results will be presented in a forthcoming paper [9].

II. EXPERIMENTAL PROCEDURE

We have taken advantage of the polarized deuteron beam available at the Laboratoire National Saturne

(LNS). Deuterons polarized in four different states called 5, 6, 7, and 8 [10] which are linear combinations of vector and tensor polarization states were accelerated sequentially in successive bursts.

The outgoing tritons labeled with the corresponding deuteron polarized state were analyzed by the high resolution spectrometer SPES 1 working in the dispersion matching mode, using the "standard" detection at the focal plane [11]. No special selection of the tritons was needed as background events were negligible.

Two scintillation telescopes, one in the reaction plane at $-45°$, the other in the vertical plane at 50°, were used to continuously monitor the beam. The counting rates were averaged over the four polarization states. The two monitors were calibrated at each energy by the carbon activation method used at the LNS [12]. The two calibrations performed at the beginning and at the end of the measurements at each incident energy were found in fair agreement (less than 10%) for the telescope placed in the vertical plane. The difference reached about 20% for the second telescope, probably due to an instability of the voltage setting. The mean results obtained with the first telescope were adopted to calculate the cross sections at the two incident energies. The statistical errors on the cross sections were a few percent or less, except for the $2p$ levels. We adopted an estimated uncertainty of 10% on the cross sections at each angle, comparable to the observed calibration shifts. An additional systematic error of about 10% on all cross sections taking into account the uncertainties on activation measurements cannot be excluded.

The vector and tensor polarization parameters ρ_{10} and ρ_{20} of the deuteron beam were periodically measured with the low energy $d(\vec{d},p)t$ polarimeter [10]. They were found to be very stable at $\rho_{10}=-0.370\pm0.015$ and $\rho_{20}=0.595\pm0.010$ which correspond typically to 90% and 85% of the maximum values of the vector and tensor polarization parameters. Calibration of the low energy polarimeter with dead time corrections may account for an additional 5% systematic errors on the deduced A_y and A_{yy} values for the relations

$$A_y=\left[\frac{2}{3}\right]^{1/2}\frac{1}{|\rho_{10}|}\frac{N_5+N_7-N_6-N_8}{\sum_i N_i},$$

$$A_{yy}=\sqrt{2}\frac{1}{|\rho_{20}|}\frac{N_5+N_6-N_7-N_8}{\sum_i N_i}.$$

The quantity A_0 defined by

$$A_0=(N_5-N_6-N_7+N_8)\Big/\left[\sum_i N_i\right],$$

and which should be zero [10], was found to be zero within a ±0.01 error, taking into account the beam polarization and assuming the same integrated number of incident deuterons on the target in each state.

The ^{208}Pb target, isotopically enriched to 99.14%, was 16.7 mg/cm^2 thick. The spectrometer slits were fixed to achieve a horizontal and vertical aperture angle of 2.4° and 2°, respectively. The scattering angle was determined to better than 0.1° in reconstructing the trajectories. For each measurement, the horizontal acceptance was divided in three intervals of 0.8° at $E_d=200$ MeV and in two intervals of 1.2° at $E_d=360$ MeV.

The measurements were performed at six angular settings of the spectrometer from 3° to 18° at $E_d=200$ MeV and from 3° to 15° at $E_d=360$ MeV. The off-line data reduction program corrects for the small dependence of the position at the focal plane on the vertical and horizontal angle of the trajectory in the spectrometer. The energy resolutions were then 120 and 140 keV at $E_d=200$ MeV and $E_d=360$ MeV, respectively, partly due to the beam transport settings, to the precision of the localization achieved by the drift chambers at the focal plane, and to the target thickness effects.

III. EXPERIMENTAL RESULTS

Typical spectra taken at $E_d=200$ and 360 MeV in the excitation region of the six valence levels are shown in Figs. 1(a) and 1(b). The $1i_{13/2}$ level dominates at both energies while the $2p$ states are very weakly excited. The two weak groups around the $\frac{9}{2}^-$ state will be discussed in a forthcoming paper together with the large number of higher-lying valence fragments with small spectroscopic factors. Special care has been taken using a peak fitting procedure to separate the pure $\frac{9}{2}^-$ state cross sections. Only the central part of the corresponding peak was taken into account in the analyzing power measurements.

At these small angles the $1h_{9/2}$ and $2f_{7/2}$ cross sections are comparable at 200 MeV while the $2f_{7/2}$ level is relatively less excited at 360 MeV, which indicates an enhanced selectivity for $l\geq5$ at 360 MeV. The experimental cross-section angular distributions are displayed in Figs. 2 and 3 at 200 and 360 MeV, respectively, for the main valence levels. The comparison of the cross sections at the smallest experimental angles shows that the $1h_{9/2}$ and $1i_{13/2}$ levels are less excited at 360 MeV than at 200 MeV by a factor of ≈4–6. This is also true for the $2f_{5/2}$ and $2f_{7/2}$ levels but the factor is then ≈15–25. The cross-section angular distributions are structureless at both energies with rather similar slopes for all levels at $E_d=360$ MeV. At $E_d=200$ MeV, the $2f$ and $2p$ levels have clearly the steepest slopes. The $1i_{13/2}$ level slope is steeper than that of the $1h_{9/2}$ level. The $l=1$ cross sections being so weak at 200 MeV and more evidently at 360 MeV, we will not discuss in the following part of this article the observables associated with these badly matched transitions.

The angular distributions of the vector and tensor analyzing powers displayed in Fig. 4 (200 MeV) and Fig. 5 (360 MeV) change drastically with the characteristics of the level. One may notice that $l-\frac{1}{2}$ transitions exhibit larger A_{yy} values than $l+\frac{1}{2}$ transitions over most of the angular range.

IV. ANALYSIS AND DISCUSSION

If $\mathbf{P}_d=\hbar\mathbf{K}_d$ and $\mathbf{P}_t=\hbar\mathbf{K}_t$ are the asymptotic momenta of the deuteron and the triton in the entrance and the exit

channels, respectively, the momentum transfer in the projectile-ejectile system in a simple plane wave calculation is defined as $q=|\mathbf{K}_d-\frac{2}{3}\mathbf{K}_t|$. At 0° this momentum transfer is about 0.9 fm^{-1} at 200 MeV and 1.4 fm^{-1} at 360 MeV. This means that at these high incident energies finite range DWBA calculations are necessary. In a recent work [13], the projectile-ejectile form factor, or range function [14], has been calculated in a consistent way; it is defined as the overlap function $\mathcal{D}(\mathbf{r})=\langle\Psi_t|V_{1n}+V_{2n}|\Psi_d\Psi_n\rangle$ where Ψ_d and Ψ_t are the deuteron and triton wave functions and Ψ_n is the spinor of the transferred neutron in the target. The nucleon-nucleon interaction V_{in} is also used to generate the deuteron and triton wave functions. The calculations of the S and D components of $\mathcal{D}(\mathbf{r})$ have been done with the Argonne [15], Urbana [16], Super Soft Core (SSC) [17], and Paris [18] potentials. It appears that, in the momentum space, $\mathcal{D}(\mathbf{q})$ is similar for each type of interaction. In the following, we will compare the present $(\vec{d},t)$ data with DWBA calculations performed with the DWUCK5 code [19] using the Paris range function. The discussion of the small differences observed with the different range functions is beyond the scope of the present paper [13].

The neutron form factors of the target nucleus were calculated by the separation energy method, choosing the Woods-Saxon geometry calculated by Mahaux [20] for the different quasihole states (typically $r_0\approx 1.22A^{1/3}$ fm for the radius and $a_0\approx 0.70$ fm for the diffuseness).

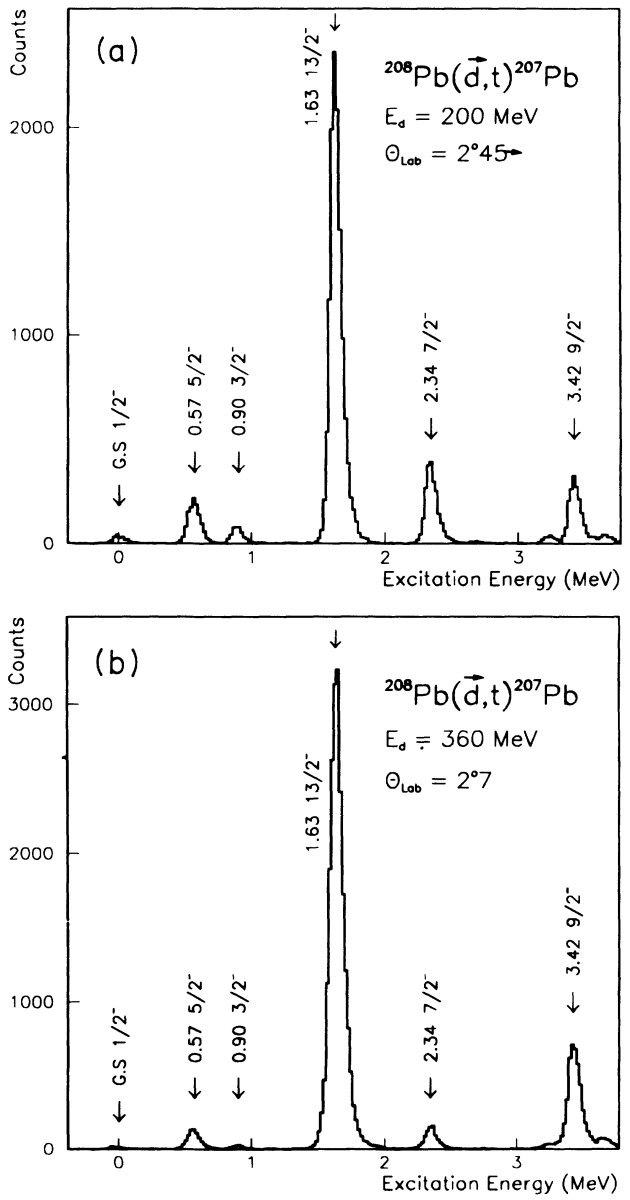

FIG. 1. ^{207}Pb excitation energy spectra at (a) $E_d=200$ MeV and (b) $E_d=360$ MeV.

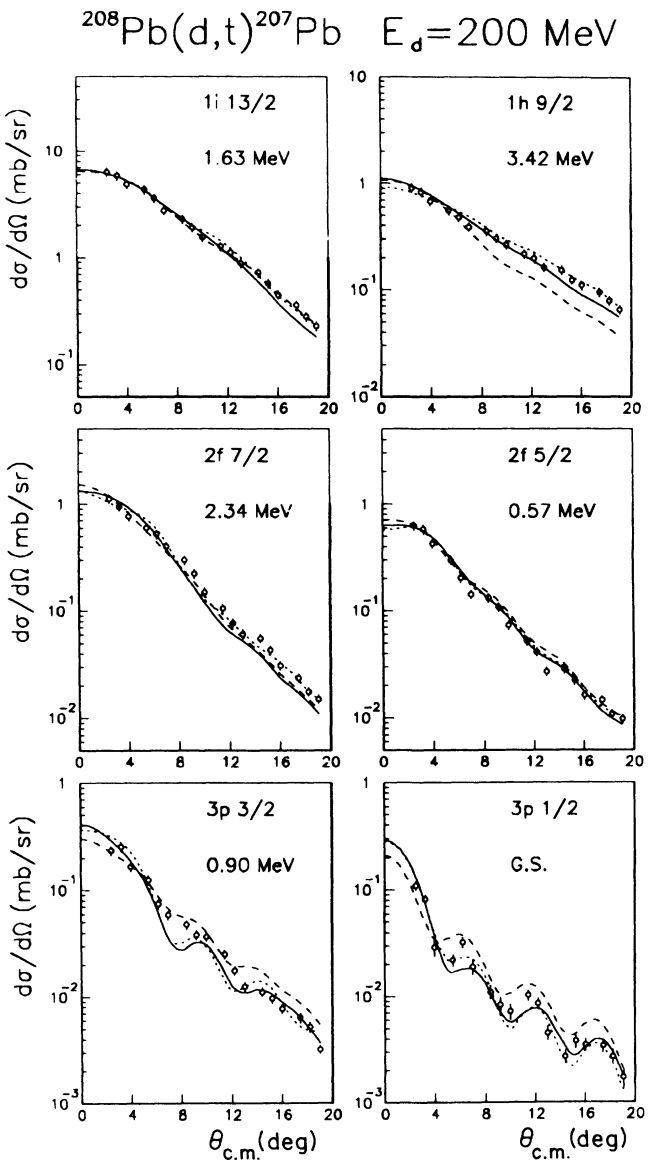

FIG. 2. Cross-section angular distributions at $E_d=200$ MeV; experimental and theoretical cross sections. Solid line: Finite range calculations with S and D components and with optical parameter set B. Dashed line: Finite range calculations with S and D components and with optical parameter set A. Dotted line: Zero-range calculations with ZR parameter set.

The influence of different optical parameters, the role of the S and D components, the transition dependence on nlj, and zero-range two-step calculations are discussed in the following paragraphs.

The optical potentials used in this analysis are not corrected for the nonlocality, which is not well known at intermediate energies. The sets A and B given in Table I correspond, respectively, to the starting and final set of optical parameters and the set ZR is used in the zero-range calculations. The spectroscopic factors for the main excited levels, deduced with the different parameter sets, are summarized in Table II.

A. Optical parameters: Adopted sets

All the analyses given in this paragraph correspond to calculations including the S and D components in the range function. At a first stage, we have used the deuteron parameters deduced from elastic scattering data previously obtained at $E_d=200$ MeV on ^{58}Ni [21] thus leading to the sets $D200A$. The parameters obtained at $E_d=400$ MeV also on ^{58}Ni [21] were slightly modified to get the parameter set $D360A$. An energy dependence estimated for nucleons at half the deuteron incident energy was used [22]. We have tried to describe the triton relative motion using the ^{3}He optical parameters deduced by Willis *et al.* [23] from their analysis of 217 MeV ^{3}He elastic scattering data. DWBA calculations with this triton optical potential could not at all reproduce the angular distributions of the measured observables at $E_d=200$ MeV. The exit channel potentials at both energies were then built on a very simplified but successful [24] adiabatic approach, by just adding neutron and proton potentials calculated at a third of the triton energies, giving the sets $T200A$ and $T360A$. The central part and the spin-orbit terms were calculated following the generalization of Keaton [25] for the $A=3$ system. The energy dependence of the parameters was taken from the systematic of Schwandt [22].

The DWBA predictions obtained at 200 MeV with the Paris interaction and the optical sets A are compared

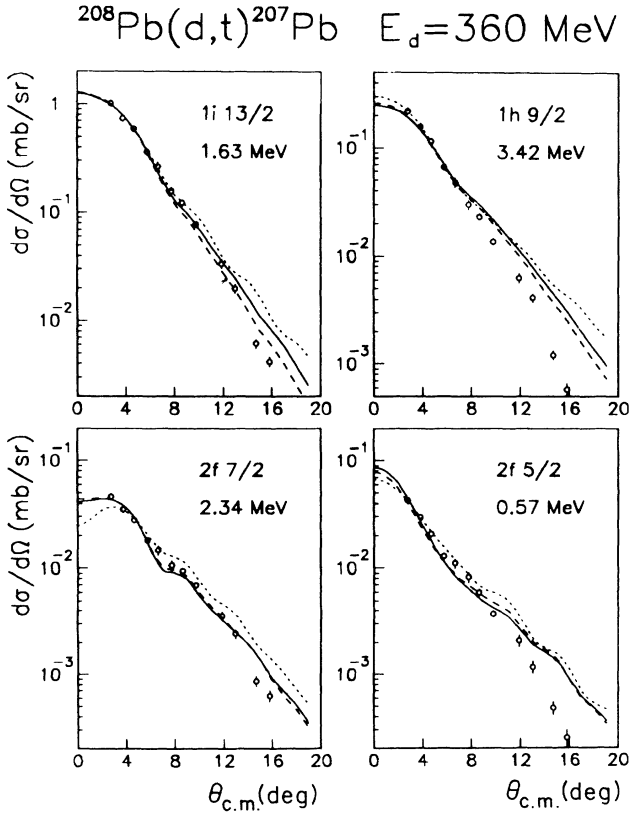

FIG. 3. Cross-section angular distributions at $E_d=360$ MeV; experimental and theoretical cross sections. Solid, dashed, and dotted lines as in Fig. 2.

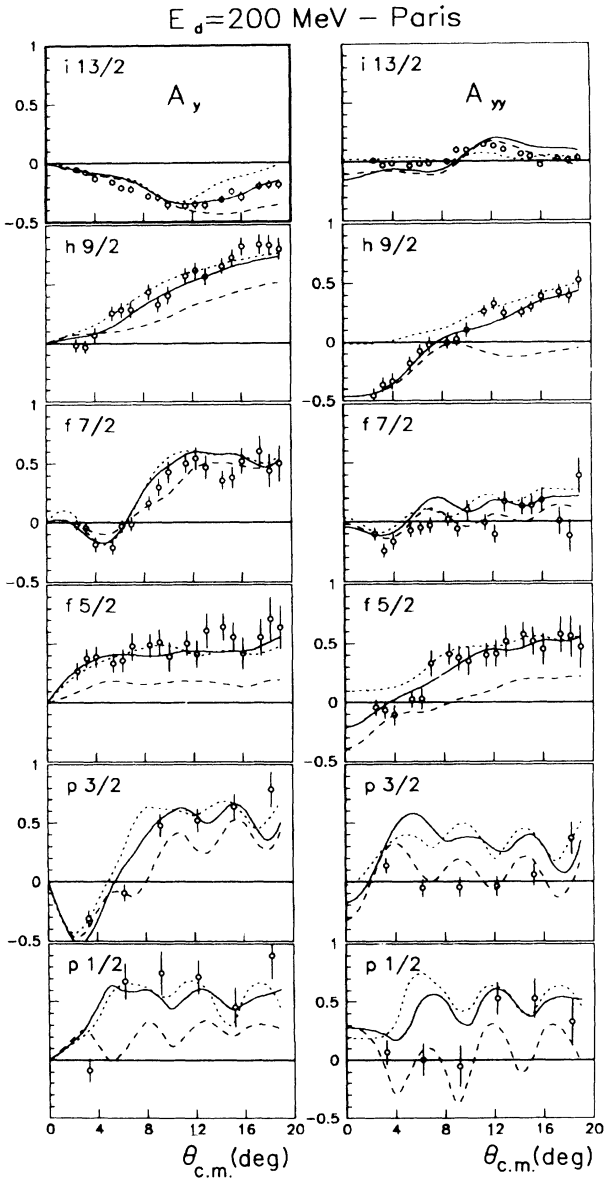

FIG. 4. Experimental and calculated analyzing powers at $E_d=200$ MeV. Solid, dashed, and dotted lines as in Fig. 2.

with the experimental angular distributions in Figs. 2 and 4. The calculations reproduce fairly well the cross-section angular distributions, except for the $1h_{9/2}$ state beyond 6°. The calculated slope of this level is slightly steeper at forward angles than that of the $1i_{13/2}$ level, contrary to the experimental data.

The calculated vector and tensor analyzing powers of the $1h_{9/2}$ and $2f_{5/2}$ levels differ strongly from the experimental data. As shown in Table II, the spectroscopic factors deduced for the $1i_{13/2}$ and $2f_{7/2}$ levels agree fairly well with the values adopted in most of the previous works, while those of the $j=l-\frac{1}{2}$ levels $1h_{9/2}$ and $2f_{5/2}$ are found somewhat smaller.

At 360 MeV the description of the A_y angular distributions using parameter set A (Fig. 5) is qualitatively good, except for the vector analyzing power of the $2f_{5/2}$ level. The shapes of the tensor analyzing powers A_{yy} are only poorly reproduced. On the other hand the slopes of the cross-section angular distributions (Fig. 3) are not well reproduced and moreover the relative spectroscopic factors, as shown in Table II, are not consistent with the values obtained at lower energies.

We tried to improve the description of the reaction, at both energies, searching for better agreement on the angular distribution shapes, and on the ratio of the $1h_{9/2}$ over $1i_{13/2}$ spectroscopic factors. The optical potentials were modified by changing the central parts or the $\mathbf{L}\cdot\mathbf{S}$ terms or by introducing a diagonal tensor term in the deuteron channel as discussed below.

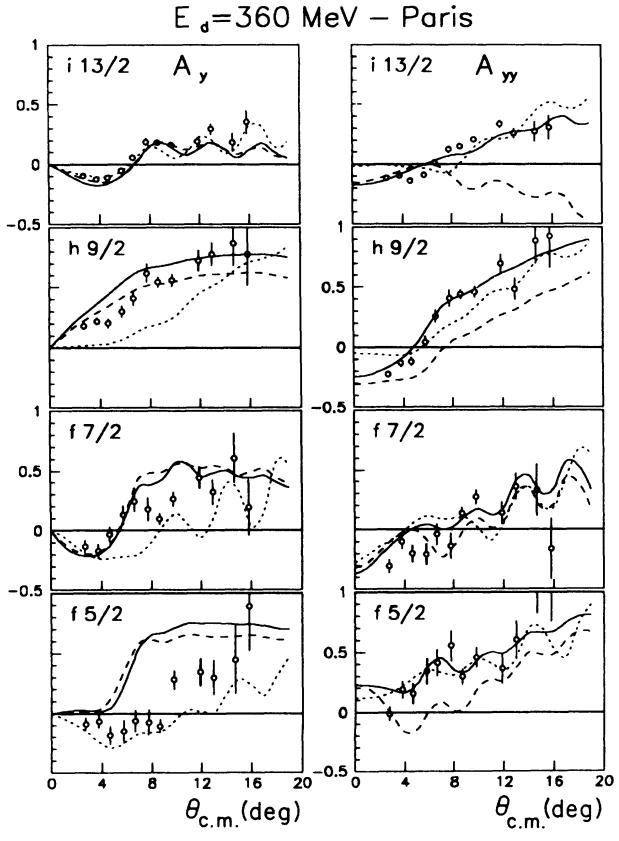

FIG. 5. Experimental and calculated analyzing powers at $E_d=360$ MeV. Solid, dashed, and dotted lines as in Fig. 2.

1. Reaction at 200 MeV

a. Central part. The effects of about 10% change on the deuteron and triton potential parameters were checked. The shape of the $1h_{9/2}$ cross-section angular distributions is significantly improved by decreasing the depth of the deuteron real potential and slightly the radius of the triton real potential (see Table I, potential set B). The ratio of the $1h_{9/2}$ and $1i_{13/2}$ spectroscopic factors increases when a larger surface thickness of the triton imaginary potential is used.

The choice of the deuteron and triton central potentials has only small effects on analyzing powers except the real depth of the deuteron potential which changes significantly the $1h_{9/2}$ tensor analyzing power beyond $\theta\approx 8°$.

b. Spin-dependent part. We checked that the spin part in the triton channel plays a minor role in the description of the observables. On the other hand we found a strong dependence on the spin part in the deuteron channel. In the analysis of their data, Nguyen *et al.* [21] obtained a good description of the three observables $d\sigma/d\Omega$, A_y, and A_{yy} with or without an imaginary term W_{ls} in the deuteron optical potential, so they chose the value $W_{ls}=0$ which we have adopted in the analysis of the $(\vec{d},t)$ reaction with the set A. However a nonzero W_{ls} term leads to an overall better description of the vector analyzing powers. The tensor analyzing powers are also improved for the $1h_{9/2}$ and $2f_{5/2}$ states but they are deteriorated for the $1i_{13/2}$ and $2f_{7/2}$ states. The addition of an imaginary diagonal tensor term W_{t_1} (with a Woods-Saxon first derivative shape) in the deuteron channel [31], the main effect of which is to increase the A_{yy} values beyond $\approx 8°$, allows a reasonable fit of both A_y and A_{yy} observables. The role of W_{ls} and W_t (Table I, set B) on analyzing powers is illustrated in Fig. 6 for the $1i_{13/2}$ and $1h_{9/2}$ states. It is interesting to notice that while the calculated values of A_y and especially A_{yy} beyond $\approx 8°$ depend on W_{ls} and W_t, this dependence is weak at the forward angles. The spin-dependent part of the deuteron channel has only slight effects on the cross-section angular distributions.

2. Reaction at 360 MeV

It is more difficult at this energy to understand in detail how the optical parameters modify the description of the reaction. We have tried, without any success, to improve the fits to the shape of the cross-section angular distributions by changing the central part of the deuteron and triton potentials. The spin part of the deuteron potential is very important to describe the A_{yy} angular distributions beyond $\approx 8°$ (see Fig. 5). With imaginary depths W_{t_1} (Woods-Saxon first derivative) and W_{t_2} (Woods-Saxon second derivative) of tensor operators (Table I, set $D360B$) we can reproduce the A_{yy} angular distributions. The spin parameters have generally small effects on A_y

TABLE I. Deuterons and tritons optical potentials.

$$V_{\text{opt}}^{\text{Nucl}}(r)=Vf(x_v)+iWf(x_w)-\left[V_{ls}\frac{1}{r}\frac{d}{dr}f(x_{vls})+iW_{ls}\frac{1}{r}\frac{d}{dr}f(x_{wls})\right]\mathbf{L}\cdot\mathbf{S}+\left[V_{t_1}f'(x_{v_{t_1}})+iW_{t_1}f'(x_{w_{t_1}})\right]T_0^0(\mathbf{L},\mathbf{S})+\left[V_{t_2}f''(x_{v_{t_2}})+iW_{t_2}f''(x_{w_{t_2}})\right]T_0^0(\mathbf{L},\mathbf{S})$$

with

$$x_n=\frac{r-R_n A^{1/3}}{A_n}\ ,\ f(x)=\frac{1}{1+e^x}\ ,\ f'(x)=\frac{d}{dx}f(x)\ ,\ f''(x)=\frac{d^2}{dx^2}f(x)\ ,$$

and

$$T_0^0(\mathbf{L},\mathbf{S})=\begin{cases}(\mathbf{L}\cdot\mathbf{S})^2+\frac{1}{2}\mathbf{L}\cdot\mathbf{S}-\frac{2}{3}\mathbf{L}^2 & \text{if } S\geq 1\ ;\\ 0 & \text{if } S<1\ .\end{cases}$$

	V (MeV)	R_v (fm)	A_v (fm)	W (MeV)	R_w (fm)	A_w (fm)	V_{ls} (MeV)	R_{vls} (fm)	A_{vls} (fm)	W_{ls} (MeV)	R_{wls} (fm)	A_{wls} (fm)	W_{t_1} (MeV)	R_{wt_1} (fm)	A_{wt_1} (fm)	W_{t_2} (MeV)	R_{wt_2} (fm)	A_{wt_2} (fm)
*D*200*A*	−41.6	1.24	0.82	−13.3	1.45	0.69	−7.8	1.08	0.77	0.0	0.0	0.0	0.0	0.0	0.0	0.0		
*D*200*B*	−36.6	1.24	0.82	−13.3	1.45	0.69	−7.8	1.08	0.77	2.0	1.2	0.6	−0.035	1.1	0.6	0.0		
*D*200*ZR*	−41.6	1.24	0.82	−13.3	1.45	0.69	−7.8	1.08	0.77	3.0	1.2	0.6	−0.03	1.1	0.6	0.0		
*T*200*A*	−98.3	1.19	0.695	−18.53	1.495	0.482	−8.23	1.038	0.672	0.35	1.016	0.62						
*T*200*B*	−98.3	1.14	0.695	−18.53	1.525	0.682	−8.23	1.038	0.672	0.35	1.016	0.62						
*T*200*ZR*	−98.3	1.19	0.695	−18.53	1.495	0.482	−8.23	1.038	0.672	0.35	1.016	0.62						
*D*360*A*	−16.24	1.35	0.733	−24.4	1.154	0.874	−7.114	1.083	0.74	0.0	0.0	0.0	0.0	0.0	0.0			
*D*360*B*	−16.24	1.35	0.733	−24.4	1.154	0.874	−7.114	1.083	0.74	2.5	1.2	0.6	−0.01	1.1	0.6	0.02	1.30	0.6
*D*360*ZR*	−16.24	1.35	0.733	−24.4	1.154	0.874	−7.114	1.083	0.74	3.0	1.2	0.6	0.005	1.1	0.6	0.02	1.2	0.6
*T*360*A*	−66.783	1.245	0.712	−23.82	1.362	0.620	−5.674	1.10	0.624	1.873	1.09	0.62						
*T*360*B*	−66.783	1.245	0.712	−23.82	1.362	0.620	−5.674	1.10	0.624	1.873	1.09	0.62						
*T*360*ZR*	−66.783	1.245	0.712	−23.82	1.362	0.620	−5.674	1.10	0.624	1.873	1.09	0.62						

TABLE II. Spectroscopic factors extracted from the ^{208}Pb($\vec{d}$,t) data at E_d=200 and 360 MeV.

		C^2S (E_d=200 MeV)			C^2S (E_d=360 MeV)			C^2S (previous works)	
Interaction		Paris		Z.R.	Paris		Z.R.	c	d
Potential set		*A*	*B*	*ZR*	*A*	*B*	*ZR*		
nlj	E_x (MeV)								
$1i_{13/2}$	1.63	9.25	10.1	10.0[a]	5.45	6.25	10.0[b]	8.5–12	4.1–11
$1h_{9/2}$	3.42	3.45	4.05	4.4	4.0	3.45	5.55	4.9–6.9	2.0–5.5
$2f_{7/2}$	2.34	5.3	5.6	4.8	4.0	4.6	4.55	4.4–7.1	3.8–8.0
$2f_{5/2}$	0.57	3.9	3.15	2.3	3.7	2.7	2.85	4.5–6.6	4.2–5.7
$3p_{3/2}$	0.9	(5.05)	(3.85)	(2.4)				2.8–7	2.8–6
$3p_{1/2}$	0	(2.1)	(1.3)	(0.7)				1.7–2.3	1.6–2.7

[a]C^2S=10.0 with a normalization factor N=1.71 (N=3.33 at low energy).
[b]C^2S=10.0 with a normalization factor N=0.87.
[c]References [26–29].
[d]Reference [30].

and σ angular distributions. However, the ratio of the $1h_{9/2}$ and $1i_{13/2}$ spectroscopic factors is improved when positive values of W_{ls} are introduced.

3. *Summary*

The best sets of optical potential parameters are the sets *B* (Table I).

At E_d=200 MeV, the angular distributions of all observables are now rather well reproduced for the six valence levels using the Paris interaction and parameter set *B* (see Figs. 2 and 4). Absolute spectroscopic factors are in reasonable agreement with the values deduced from previous works (see Table II).

At 360 MeV, set *B* and set *A* differ only by the imaginary **L·S** and diagonal tensor terms of the deuteron potential. The improvement bears on the relative spectroscopic factors (see Fig. 3 and Table II) and on the description of the shapes of the tensor analyzing powers.

The DWBA angular distributions of the three observables in the forward angle region appear little or not sensitive to the optical potentials, within some 10% variation of the parameters.

One notices that elastic scattering angular distributions calculated with potential sets *A* and *B* are found very similar for the cross section up to ≈20°. This is also true to a lesser extent for the analyzing powers.

B. Effect of the *D* component in the range function

It is expected that finite range effects and, more precisely, the contribution of the *D* state in the range function, become more important as the incident energy increases. The influence of the *D* component is discussed at both energies for the strongly excited $1h_{9/2}$ and $1i_{13/2}$ levels.

At E_d=200 MeV, including or not the *D* component in the calculation, absolute cross sections of the different states remain nearly the same except for the $1h_{9/2}$ level. In that case, the cross section at the smallest angles increases of 18% while the slope of the cross-section angular distribution increases significantly if the *D* component is included. As shown in Fig. 7 for the $1i_{13/2}$ and $1h_{9/2}$ levels, the effect of the *D* component is negligible on A_y. The effect is also negligible on A_{yy} beyond ≈8° but quite important at forward angles, especially for the $1h_{9/2}$ level.

At 360 MeV, the theoretical cross sections increase at forward angles by 22% for the $1h_{9/2}$ level and 4% for the $1i_{13/2}$ level when the *D* component is included in the DWBA calculations. Also at forward angles, the *D* state contribution is responsible for the good agreement achieved with the A_{yy} data both for the $1i_{13/2}$ and $1h_{9/2}$ levels, as shown in Fig. 8. The vector analyzing powers calculated with and without the *D* state are very similar.

C. Transition dependence on *nlj*

We have emphasized in Sec. III that at E_d=200 MeV the cross-section angular distributions have different

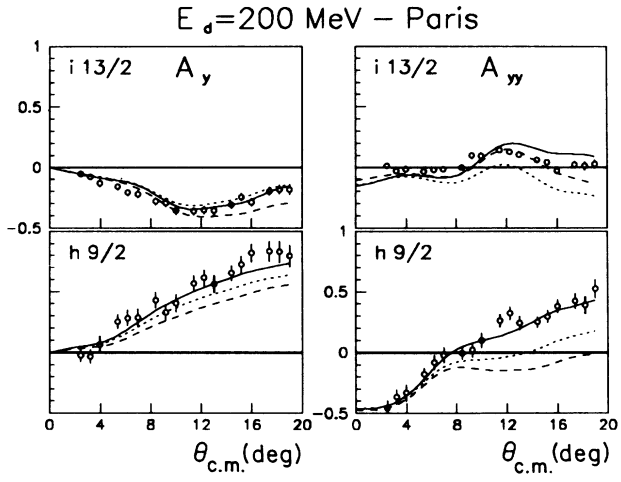

FIG. 6. Dependence of A_y and A_{yy} on the spin part of the deuteron optical potential; finite range calculations with *S* and *D* components. Solid line: Optical parameter set *B*. Dashed line: Optical parameter set *B* except $W_{ls}=W_t=0$. Dotted line: Optical parameter set *B* except $W_t=0$.

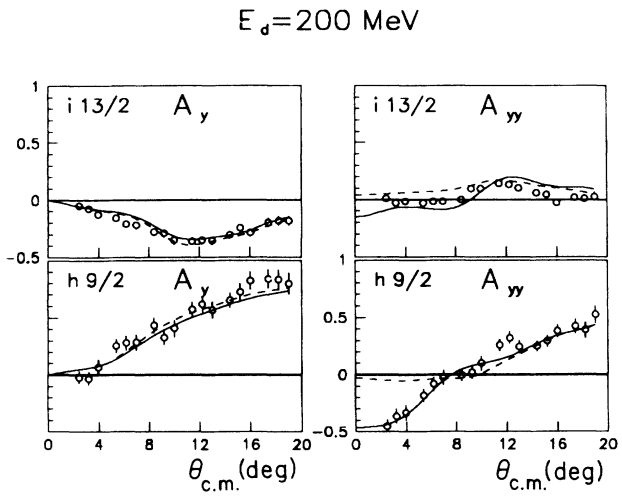

FIG. 7. $E_d=200$ MeV: Dependence of A_y and A_{yy} on the S and D components. Finite range calculations with parameter set B. Solid line: S and D components. Dashed line: S component only.

slopes for the $1i_{13/2}$, $1h_{9/2}$, and $2f$ levels, which is not the case at $E_d=360$ MeV. At both energies, angular distributions of the vector and tensor analyzing powers exhibit strong characteristic features. In order to understand the specific role of the nlj quantum numbers, DWBA calculations have been performed at $E_d=200$ MeV for several inner hole states such as $1h_{11/2}$, $1g_{7/2}$, $2d_{5/2}$, $2d_{3/2}$, and $1g_{9/2}$ using separation energies calculated by Mahaux [20].

The behavior of the three observables is found strikingly similar for hole states with different l values but with the same number of nodes and the same spin and angular momentum coupling $j_+=l+\frac{1}{2}$ or $j_-=l-\frac{1}{2}$. Typical calculations for the analyzing powers are presented in Fig. 9. This similarity remains qualitatively true if the hole state energy is changed by several MeV and if DWBA calculations are performed at $E_d=360$ MeV. A weak dependence on l, a significant dependence on n, and a strong dependence on the j_+ or j_- type of states have previously been noticed in a systematic survey of $(\vec{p},d)$ analyzing powers measured over a large range of nuclei at 65 MeV incident energy [32]. No n dependence has been found in another systematic study of the same reaction at higher incident energy [5].

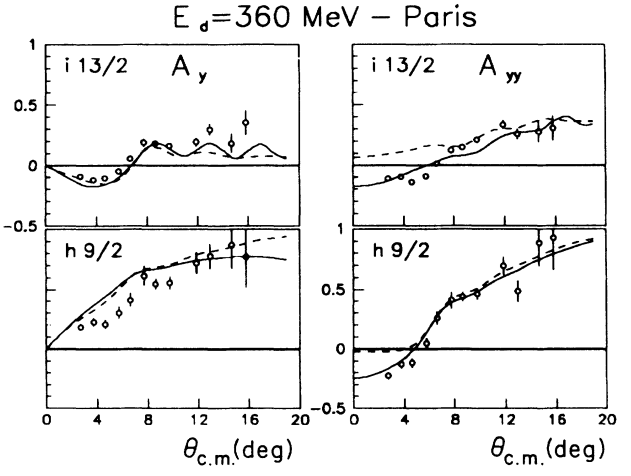

FIG. 8. $E_d=360$ MeV: Dependence of A_y and A_{yy} on the S and D components; finite range calculations with parameter set B. Solid line: S and D components. Dashed line: S component only.

D. Zero-range calculations and two-step process effects

As indicated in Sec. IV B, the contribution of the D part of the range function, except for the description of tensor analyzing powers at forward angles, plays a rather limited role in the $(\vec{d},t)$ reaction at $E_d=200$ MeV and even at $E_d=360$ MeV. Under these conditions, zero-range calculations may offer a simple and convenient approach to describe many features of the reaction. The agreement achieved with angular distribution data of the three observables and using the set ZR is illustrated in Figs. 2–5. Adopting $C^2S=10$ for the $li_{13/2}$ level, the normalization factors are $N=1.71$ at $E_d=200$ MeV and $N=0.87$ at $E_d=360$ MeV instead of the usual value $N=3.33$. The ratio of the $1h_{9/2}$ to $li_{13/2}$ level spectroscopic factors is well reproduced at both energies while the mean value of the $1f_{7/2}$ over $1f_{5/2}$ spectroscopic factors is found too small at $E_d=360$ MeV (see Table II). In

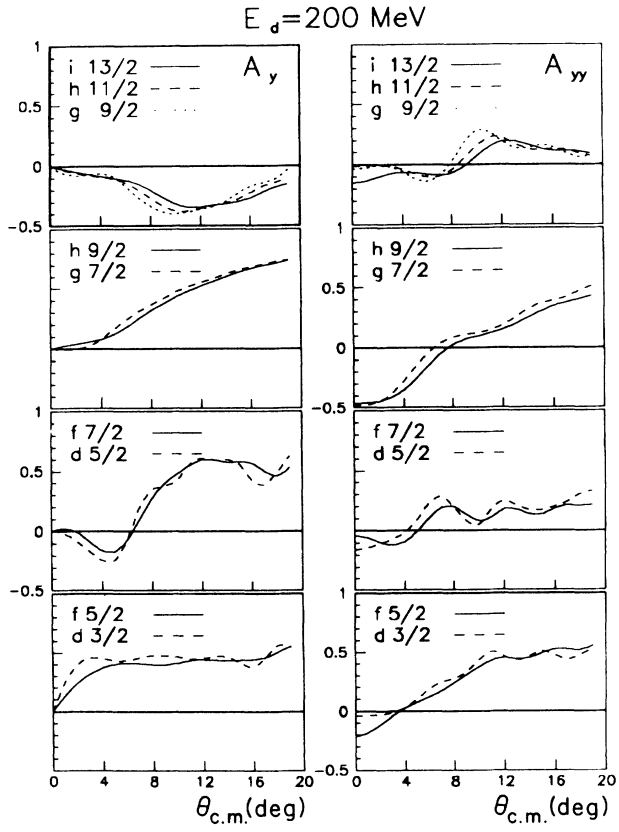

FIG. 9. $E_d=200$ MeV: Dependence of A_y and A_{yy} on nlj.

order to evaluate two-step pick up cross sections related to the first 3^- collective vibration in ^{208}Pb, zero-range calculations have been performed with the code CHUCK [19] modified in order to introduce tensor and imaginary **L·S** components in the deuteron potential. Maximum cross sections reaching about 20–50 μb at the two incident energies are found negligible for the strongly excited $1i_{13/2}$ level and would at most change the deduced $1h_{9/2}$ and $2f_{7/2}$ level spectroscopic factors by typically 10% and 25% at both energies.

V. SUMMARY AND CONCLUSIONS

Differential cross sections, vector and tensor analyzing powers have been measured for the first time in a $(\vec{d},t)$ reaction induced by a high incident energy beam. The reaction ^{208}Pb$(\vec{d},t)^{207}$Pb at $E_d=200$ and 360 MeV populates selectively the higher l transfer transitions among the valence hole states. The experimental cross-section angular distributions are structureless but both spin observables A_y and, to a lesser extent A_{yy}, allow a clear identification, especially at 200 MeV, of these well-known valence levels taken as a reference. The j_- analyzing powers have, on the average, larger absolute values than the j_+ analyzing powers.

The data have been systematically compared with exact finite range calculations using the Paris interaction. An overall good agreement could be achieved for all three observables $d\sigma/d\Omega$, A_y, and A_{yy} and the four main valence levels at $E_d=200$ MeV. The description of the reaction is only qualitative at $E_d=360$ MeV.

We emphasize the following conclusions.

(i) At both energies, the D component in the DWBA calculation has significant effects on the relative cross sections of j_- vs j_+ levels at forward angles. Also at forward angles, it is necessary to describe tensor analyzing powers. Its effect on A_y is small over the whole angular range.

(ii) The spin part of the deuteron optical potential is very important to describe the analyzing power angular distributions at both energies over most of the measured angular range. An imaginary diagonal tensor term has been introduced in order to better reproduce the A_{yy} angular distributions beyond 8°. At $E_d=360$ MeV relative spectroscopic factors are improved when an imaginary **L·S** term is included in the calculation.

The $(\vec{d},t)$ reaction at $E_d=200$ MeV appears as a good spectroscopic tool to study the fragmentation of high l neutron hole states in heavy nuclei. The measurement of vector analyzing powers is most important in this respect, as they exhibit the largest differences between the j_- and j_+ states and they are less sensitive to the optical potential parameters. Tensor analyzing powers give useful additional information. The measurement of that observable at the smallest angles, where cross sections are large but vector analyzing powers generally small, is of special interest.

Further experiments and theoretical efforts are needed for a better understanding of the $(\vec{d},t)$ reaction at intermediate energies. In particular, an experimental survey of the dependence on nlj of the three observables $d\sigma/d\Omega$, A_y, and A_{yy}, using known states in other nuclei, would be most interesting. Theoretical approaches to the role of the coupling of the deuteron and triton to the breakup continuum would be most valuable. Nonlocality and relativistic effects remain to be studied.

ACKNOWLEDGEMENTS

The authors are indebted to J. C. Duchazeau-Beneix and J. C. Lugol for their help during the experiment. We would like to thank the technical staff of the Laboratoire National Saturne for its efficient assistance.

[1] S. Galès, Ch. Stoyanov, and A. I. Vdovin, Phys. Rep. **166**, 125 (1988), and references therein.

[2] M. C. Radhakrishna, N. G. Puttaswamy, H. Nann, J. D. Brown, W. W. Jacobs, W. P. Jones, D. W. Miller, P. P. Singh, and E. J. Stephenson, Phys. Rev. C **37**, 66 (1988).

[3] Swapan K. Saha, W. W. Daehnick, S. A. Dytman, P. C. Li, J. G. Hardie, G. P. A. Berg, C. C. Foster, W. P. Jones, D. W. Miller, and E. J. Stephenson, Phys. Rev. C **40**, 39 (1989); **42**, 922 (1990); K. Reiner, P. Grabmayr, G. J. Wagner, S. M. Banks, B. G. Lay, V. C. Officer, G. G. Shute, B. M. Spicer, C. W. Glover, W. P. Jones, D. W. Miller, H. Nann, and E. J. Stephenson, Nucl. Phys. **A472**, 1 (1987).

[4] J. Kasagi, G. M. Crawley, E. Kashy, J. Duffy, S. Galès, E. Gerlic, and D. Friesel, Phys. Rev. C **28**, 1065 (1983).

[5] H. Nann, D. W. Miller, W. W. Jacobs, D. W. Devins, W. P. Jones, and Li Qing-Li, Phys. Rev. C **27**, 1073 (1983).

[6] R. Abegg, D. A. Hutcheon, C. A. Miller, L. Antonuk, J. M. Cameron, G. Gaillard, J. M. Kitching, R. P. Liljestrand, W. J. McDonald, W. C. Olsen, G. M. Stinson, J. Tinsley, and P. D. Kunz, Phys. Rev. C **39**, 65 (1989).

[7] C. M. Bhat, J. E. Bowsher, T. B. Clegg, H. J. Karwowski, E. J. Ludwig, and B. A. Brown, Phys. Rev. C **38**, 1537 (1988); C. M. Bhat, E. J. Ludwig, T. B. Clegg, and H. J. Karwowski, Nucl. Phys. **A526**, 36 (1991).

[8] H. Langevin-Joliot, E. Gerlic, J. Guillot, M. Sakai, J. Van de Wiele, A. Devaux, P. Force, and G. Landaud, Phys. Lett. **114B**, 103 (1982), and references therein.

[9] H. Langevin-Joliot *et al.* (unpublished); J. Van de Wiele *et al.*, IPN Annual Report 97, 1990.

[10] J. Arvieux, S. D. Baker, A. Boudard, J. Cameron, T. Hasegawa, D. Hutcheon, C. Kerboul, G. Gaillard, and Nguyen Van Sen, Nucl. Instrum. Methods **A273**, 48 (1988).

[11] R. Beurtey, Summer School, Nuclear and Particle Physics at Intermediate Energies, Brentwood College School, British Columbia, Canada, 1975 (unpublished); J. Saudinos, J. C. Duchazeaubeneix, C. Laspalles, and R. Chaminade, Nucl. Instrum. Methods **11**, 77 (1973).

[12] H. Quechon, Thèse d'Etat, Université Paris XI, Orsay, 1980; J. Radin, H. Quechon, G. M. Raisbeck, and F. Yiou, Phys. Rev. C **26**, 2565 (1982).

[13] J. L. Ballot, J. Van de Wiele, and G. Cory (unpublished); J. Van de Wiele, IPN Annual Report 78, 1989.

[14] N. S. Chant and J. N. Craig, Phys. Rev. C **14**, 1763 (1976).
[15] R. B. Wiringa, R. A. Smith, and T. L. Ainsworth, Phys. Rev. C **29**, 1207 (1984).
[16] I. E. Lagaris and V. R. Pandharipande, Nucl. Phys. **A359**, 331 (1981).
[17] R. De Tourreil and D. W. Sprung, Nucl. Phys. **A201**, 193 (1973).
[18] M. Lacombe, B. Loiseau, J. M. Richard, R. Vinh Mau, J. Cote, P. Pires, and R. De Tourreil, Phys. Rev. C **21**, 861 (1990).
[19] P. D. Kunz, University of Colorado, Boulder, CO (unpublished).
[20] C. Mahaux and R. Sartor, Nucl. Phys. **A493**, 157 (1989), and references therein.
[21] Nguyen Van Sen, J. Arvieux, Ye Yanlin, G. Gaillard, B. Bonin, A. Boudard, G. Bruge, J. C. Lugol, R. Babinet, T. Hasegawa, F. Soga, J. M. Cameron, G. C. Neilson, and D. M. Sheppard, Phys. Lett. **156B**, 185 (1985).
[22] P. Schwandt, H. O. Meyer, W. W. Jacobs, A. D. Bacher, S. E. Vigdor, M. D. Kaitchuck, and T. R. Donoghue, Phys. Rev. C **26**, 55 (1982).
[23] N. Willis, I. Brissaud, Y. Le Bornec, B. Tatischeff, and G. Duhamel, Nucl. Phys. **A204**, 454 (1973).
[24] J. Guillot, H. Langevin-Joliot, J. Van de Wiele, E. Gerlic, J. J. Florent, A. Willis, G. Duhamel-Chretien, and E. Hourani, Phys. Lett. B **258**, 271 (1991).
[25] P. W. Keaton, Jr. and D. D. Armstrong, Phys. Rev. C **8**, 1692 (1973).
[26] J. Guillot, J. Van de Wiele, H. Langevin-Joliot, E. Gerlic, J. P. Didelez, G. Duhamel, G. Perrin, M. Buenerd, and J. Chauvin, Phys. Rev. C **21**, 879 (1980).
[27] S. Galès, G. M. Crawley, D. Weber, and B. Zwieglinski, Phys. Rev. C **18**, 2475 (1978).
[28] S. M. Smith, P. G. Roos, C. Moazed, and A. M. Bernstein, Nucl. Phys. **A173**, 32 (1971).
[29] W. A. Lanford and G. M. Crawley, Phys. Rev. C **9**, 646 (1974).
[30] S. A. Dickey, J. J. Kraushaar, and M. A. Rumore, Nucl. Phys. **A391**, 413 (1982).
[31] Y. Iseri, M. Tanifuji, H. Kameyama, M. Kamimura, and M. Yahiro, Reports on the workshop on polarized nuclear reaction Ibaraki, Japan, 1990 (unpublished); Y. Iseri, M. Tanifuji, Y. Aoki, and M. Kawai, Phys. Lett. B **265**, 207 (1991).
[32] K. Hosono, M. Kondo, T. Saito, N. Matsuoka, N. Nagamachi, T. Noro, H. Shimizu, S. Kato, K. Okada, K. Ogino, and Y. Kadota, Nucl. Phys. **A343**, 234 (1980).